Check for updates

Importance of molecular symmetry for enantiomeric excess recognition by NMR†‡

Karolis Norvaiša, [ID] [a] John E. O'Brien,[b] Irina Osadchuk, [ID] [c] Brendan Twamley,[b] Victor Borovkov [ID] [c] and Mathias O. Senge [ID] *[ad]

Recently prochiral solvating agents (*pro*-CSA) came under the spotlight for the detection of enantiopurity by NMR. Chemical shift non-equivalency in achiral hosts introduced by the presence of chiral guests yields observable resonance signal splitting ($\Delta\delta$) correlating to the enantiomeric excess (e.e.). In this work, symmetry is our lens to explain porphyrin-based supramolecular receptor activity in a chiral environment. Based on extensive NMR analyses of the atropisomeric receptors, the host symmetry is shown to be affected by porphyrin nonplanarity and further desymmetrized in the presence of a chiral guest. As such, the exposed porphyrin inner core (N–H), with its strong hydrogen bond abilities, for the first time, has been exploited in enantiomeric composition analysis. Our approach in e.e. detection by N–H signals appearing in a previously underutilized region of the spectrum (below 0 ppm) shows chemical shift splitting ($\Delta\delta$) three times more sensitive to enantiomeric compositions than previously reported systems.

Among the numerous stereodiscrimination methods, nuclear magnetic resonance (NMR) spectroscopy continues to be one of the leading tools for determining the enantiomeric purity of chiral molecules.[1] Recently, a new type of NMR spectroscopic detection of enantiomeric excess (e.e.) using prochiral solvating agents (*pro*-CSA) was introduced by Hill and co-workers.[2]

[a] *School of Chemistry, Chair of Organic Chemistry, Trinity Biomedical Sciences Institute, 152–160 Pearse Street, Trinity College Dublin, The University of Dublin, Dublin 2, Ireland*

[b] *School of Chemistry, Trinity College Dublin, The University of Dublin, Dublin 2, Ireland*

[c] *Department of Chemistry and Biotechnology, Tallinn University of Technology, Akadeemia tee 15, Tallinn 12618, Estonia*

[d] *Institute for Advanced Study (TUM-IAS) Technical University of Munich, Focus Group – Molecular and Interfacial Engineering of Organic Nanosystems, Lichtenbergstrasse 2a, D-85748 Garching, Germany. E-mail: mathias.senge@tum.de; Web: www.twitter.com/mathiassenge, https://www.sengegroup.eu/*

† A previous version of this manuscript has been deposited on a preprint server (https://doi.org/10.26434/chemrxiv-2022-xg9bd).

‡ Electronic supplementary information (ESI) available: CCDC 2143572 (for $\alpha_2\beta_2$-$\mathbf{P}[SO_4{}^{2-}][HSO_4{}^-]_4$). For ESI and crystallographic data in CIF or other electronic format see DOI: https://doi.org/10.1039/d2cc01319c

In principle, in the event of attractive noncovalent physico-chemical interactions, the chiral information of a guest can be transferred to an achiral host and detected as the splitting of the NMR signals. The key example of *pro*-CSA, *N*,*N'*-disubstituted oxoporphyrinogen (**Bz₂oxP**) exhibits a linear response between the e.e. value and the magnitude of β-proton splitting ($\Delta\delta$) in ^{1}H NMR (Fig. 1a).[3] Due to *N*-alkylation of the **Bz₂oxP** core, the system cannot be protonated and hence suffers serious sensitivity issues compared to un-modified **oxP**. However, the inevitable prototropic tautomerism and macrocyclic inversions obstruct the potential applications of **oxP** as a *pro*-CSA.[2a,4] Porphyrins, as prospective *pro*-CSA candidates for e.e. detection, have also been investigated.[5] While 5,10,15,20-tetraphenylporphyrin (**TPP**) is not affected by the disadvantageous tautomeric processes, as opposed to **oxP**, the necessary use of low temperatures for the e.e. detection limits the analysis to explicit solvents with a low freezing point (*e.g.* CDCl₃) and analyte solubility during the screening (*e.g.* precipitation).

Frequently, the use of *pro*-CSA's ^{1}H NMR spectra for chiral analysis is severely hampered due to the numerous scalar couplings and overlapping signals that lead to analytical difficulties.[6] As the majority of organic molecule resonances appear between 0–14 ppm in the ^{1}H NMR scale,[7] it is desirable that the e.e. monitoring with *pro*-CSA would be in a distinct, well-separated region. One of the most unique characteristics of porphyrins is the closed-loop of electrons (ring current) exhibiting large magnetic anisotropy under an applied magnetic field. While peripheral macrocycle signals relate to the typical organic resonances, the nuclei positioned within the loop experience a strong shielding effect when subjected to an external magnetic field and resonate below 0 ppm in the ^{1}H NMR scale.[8] Once the highly conjugated system is disrupted (*e.g.*, in oxoporphyrinogens, calix[4]pyrroles), the anisotropic shielding effect of the inner core system is lost, resulting in downfield shifting of the corresponding inner core signals.

The attractive features of the metal-free (free base) porphyrin inner core has lately drawn attention in the fields of catalysis,[9]
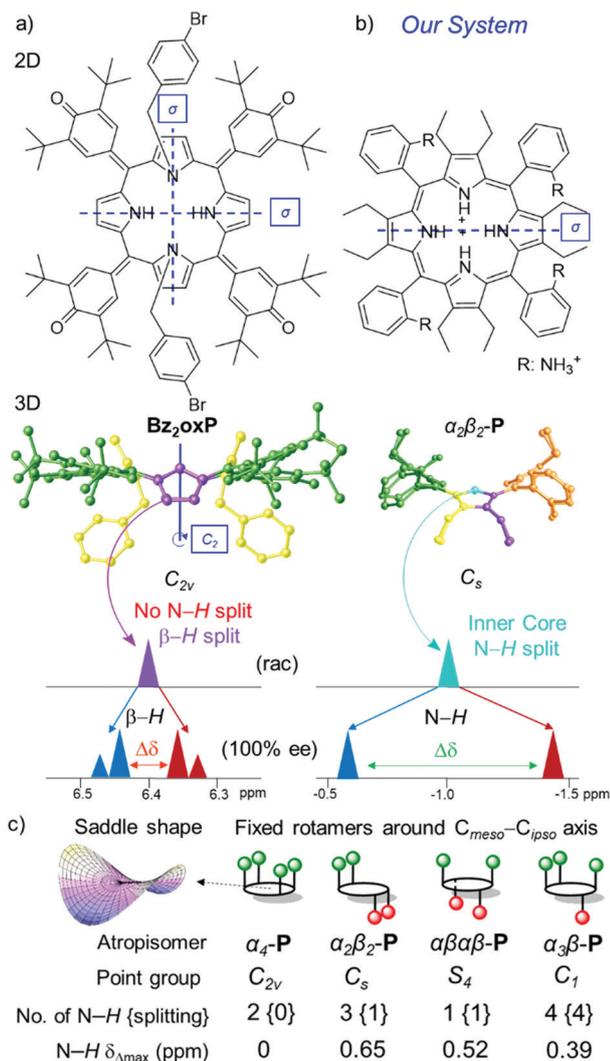
Fig. 1 2D (top view) and 3D (side view) representation of *pro*-CSA's with symmetry elements (mirror plane σ and rotation axis C_n), color coding of symmetrical groups, and the key units used for e.e. detection by ^{1}H NMR in (a) **Bz₂oxP** highlighting β–*H* splitting;[3] (b) newly designed α₂β₂-**P** receptor system with chiral discrimination by N–*H*; (c) All possible **P** atropisomers with corresponding point groups (note, the symmetry is reduced due to the saddle shape of the macrocycle), N–H signals, and magnitude of splitting; see more detail in Fig. S1 (ESI‡).

sensing,[10] supramolecular assemblies,[11] and absolute configuration determination.[12] The existing methods of ring puckering by steric strain[13] can cause a degree of outwards orientation of the inner pyrrolic entities, making these positions more basic[14] and accessible to substrates.[10] Even though porphyrins adopt a saddle-shaped 3D conformation[15] creating an 'active center' in the core, only the saddle-deformation alongside chiral guest interactions is not enough to drive the inner N–H signal to split during the ^{1}H NMR e.e. analysis. For example, **Bz₂oxP** has a saddle shape and belongs to the C_{2v} point-group notation with two mirror planes diagonally dividing all pyrroles (Fig. 1a). The symmetrical nature of **Bz₂oxP** does not permit the e.e. discrimination using the inner core and remain isochronous.[3]

Here we report the first example of e.e. detection using porphyrin inner core N–H resonances. We have designed **P** [5,10,15,20-tetrakis(2-aminiumphenyl)-2,3,7,8,12,13,17,18-octaethylporphyrin] as a receptor system (Fig. 2a) exploiting three main molecular engineering strategies: (1) steric overcrowding to obtain a saddle-shaped macrocycle while retaining the porphyrin conjugation[13] and exposing the inner pyrrolic units for host–guest interactions; (2) peripheral donating groups creating a lock-and-key[10a] comparable system to encapsulate chiral analytes in the porphyrin lattice and allow detailed NMR analysis at room temperature;[10b] (3) formation of atropisomers based on the orientation of peripheral groups[16] to have ultimate control of the symmetry elements in *pro*-CSA.[17]

Previously, we have shown the separation of atropisomers and highlighted selective nature of host **P** for guests containing sulfonate or phosphonate motifs.[10b] The analyte interacts directly with the inner ring system and generates static and well-resolved NMR spectral lines.[17] As mentioned, low temperatures can also offer slow exchange rates for potential detection of e.e.[5] However, the aim of the following studies is the development of a readily available and highly effective analytical tool for room-temperature measurements. Hence, (±)-10-camphorsulfonic acid (**10CSA**) bearing the sulfonic moiety and stereogenic centers was selected as a chiral guest.

Operating with enantiopure **10CSA**(**S** or **R**) four distinct scenarios with four different **P** atropisomers were observed and subsequently rationalized by the symmetry operations found in **P** (Fig. 1c).[17] In the α₄-**P**·**10CSA**(**S** or **R**) complex, the inner core remains isochronous, due to the C_{2v} point-group notation with a two-fold symmetry axis and two mirror planes passing through the pyrroles. The identical situation previously reported by Hill and co-workers in **Bz₂oxP** pinpoints the interactions with inner N–H, however, without the e.e. discrimination due to the C_{2v} symmetry (Fig. 1a).[3] The α₂β₂-**P** atropisomer with C_s symmetry features a single well-defined mirror plane dividing two pyrrolic units which preserve its achiral nature; hence, allowing it to be classified as *pro*-CSA. The lack of other symmetry elements in α₂β₂-**P** allows the N–H protons to become anisochronous in a chiral environment, making chiral discrimination possible (with the highest magnitude of splitting ($\Delta\delta_{max}$) of 0.653 ppm at 100% e.e.) (Fig. 1b). The α₃β-**P** atropisomer belongs to the C_1 point-group, as it contains no symmetry elements, making the system chiral. Thus, eight signals are observed with enantiopure **10CSA** due to diastereomer formation (*SS*- and *SR*- or *RR*- and *RS*-) (Fig. S1, ESI‡).

While the e.e. detection is possible with α₃β-**P** (Fig. S2, ESI‡), the practical use of such system falls short mainly due to three dominating factors: (1) the high number of inner core system signals hampers direct e.e. interpretation; (2) the magnitude of $\Delta\delta_{max}$ ($\sim$0.39 ppm) is lowest of the three atropisomers with inner core splitting making it the least sensitive system; (3) the concentration of α₃β-**P** is required to be significantly higher than that of other systems due to a large number of resonance signals and their comparatively lower intensities. On the other hand, αβαβ-**P** which belongs to the S_4 point group has four equivalent protons located in the principal axis. While it has no
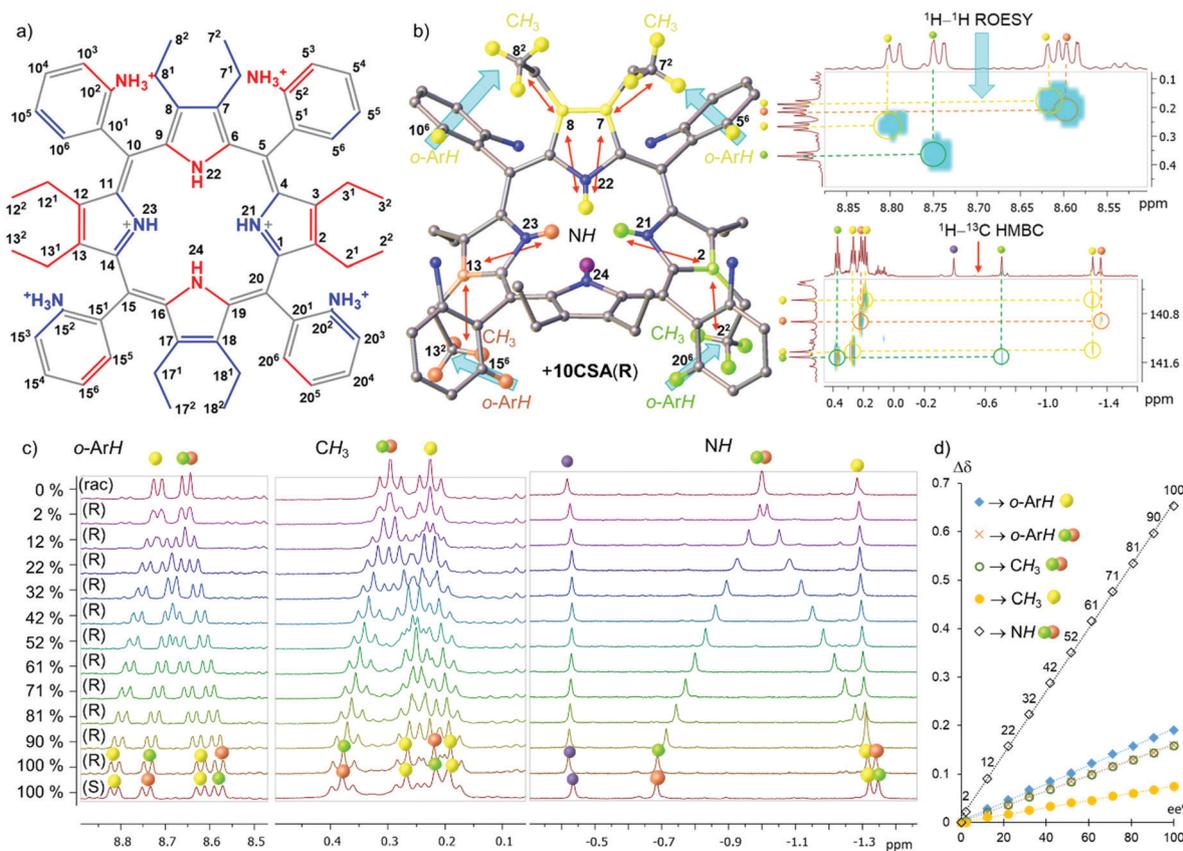
Fig. 2 (a) Illustration of the structure of $\alpha_2\beta_2$-**P** (blue – above and red – below the plane) with corresponding positions; (b) representation and color-coding reference of the ^{1}H splitting signals with blue arrows showing ^{1}H–^{1}H ROESY and red arrows ^{1}H–^{13}C HMBC correlations of 20 eq. $\alpha_2\beta_2$-**P**·**10CSA(R)**; (c) observable $\Delta\sigma$ of ^{1}H signals in o-ArH, CH_3, and inner core system (NH) regions; (d) graph of the $\Delta\sigma$ dependence on the e.e.% value. All spectra have been recorded in CD$_3$CN.

mirror planes, the inversion center situated between the pyrrole units allows the inner core protons to split in equal proportions (above and below the plane) upon interaction with a chiral analyte. A single isochronous N–H signal of $\alpha\beta\alpha\beta$-**P**-**10CSA(S** or **R)** becomes anisochronous, with $\Delta\delta_{max}$ (0.520 ppm) comparable to the $\alpha_2\beta_2$-**P**·**10CSA(S** or **R)** system (0.653 ppm). While a singular inner core proton splitting is an attractive feature, the practicality of such a system in the e.e. detection is challenging, mainly due to the low atropisomeric rotational barrier, which leads to the formation of other atropisomers at room temperature[10b] and low abundancy (only 1/8 obtained from statistical mixtures) in comparison to other **P** rotamers. Since $\alpha_2\beta_2$-**P** displayed the highest $\Delta\sigma_{max}$ value compared to other **P** atropisomeric species (Fig. 1c), in-depth chirality determination studies listed below were carried out with this receptor system (Fig. 2).

Overall, three distinct and well-resolved regions (o-ArH, CH_3, and N–H) were identified for possible e.e. monitoring with $\alpha_2\beta_2$-**P** (Fig. 2c and Fig. S5, ESI‡). The correlation between the signals of interest was investigated by 2D NMR techniques with enantiopure **10CSA(R)** (20 eq.) and their corresponding locations are illustrated in Fig. 2b. The gradual addition of **10CSA(R)** to $\alpha_2\beta_2$-**P** and the influence of water on $\Delta\sigma_{max}$ as a competitive agent is

detailed in the ESI‡ (Fig. S3–S9). While the $\Delta\sigma_{max}$ values of o-ArH and CH_3 are comparable to known pro-CSAs[2–5,18] being 0.190 ppm (o-ArH yellow), 0.159 ppm (o-ArH red/green), 0.158 ppm (CH_3 red/green), and 0.075 ppm (CH_3 yellow), the $\Delta\sigma_{max}$ values of the inner system (N–H red/green) was found to be more than threefold greater than those of other regions (0.653 ppm).

Since the $\Delta\sigma_{max}$ value of the inner core system is substantially higher than that of other regions, the resolution, of which e.e. can be detected, is considerably enhanced. Astonishingly, at as low as 2% e.e., two distinct N–H resonance singlets ($\Delta\sigma$ 0.022 ppm.) can clearly be identified, while the other regions show only a broadening of the signals. Plotting the differences in the chemical shifts of split peaks against the % e.e. values revealed a linear dependency with the R^2 values being above 0.997 and the inner N–H fitting R^2 = 0.9994 (Fig. 2d). The linear fit of the plots is a fundamental property in unlocking the easy calibration of the referenced systems for quick detection of the e.e. value (a detailed example shown in ESI;‡ Fig. S10–S12). Moreover, spatially distant neighboring protons from N–H offer another important feature. Sharp and well-isolated singlets do not suffer from any vicinal scalar J-couplings or roofing effects underlining the simplicity in tracking chiral compositions.
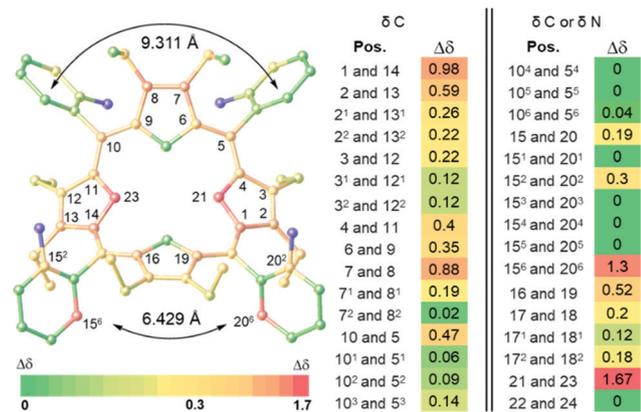
Fig. 3 Illustration of $\Delta\sigma_{max}$ (ppm) of ^{13}C and ^{15}N NMR in 20 eq. $\alpha_2\beta_2$-**P-10CSA(S)** complex, determined in comparison to the corresponding racemate $\alpha_2\beta_2$-**P-10CSA(SR)** using 2D NMR techniques (CD$_3$CN) (Fig. S16–S31, ESI‡). The highlighted positions in the illustration on the left side shows $\Delta\sigma \geq 0.3$ ppm. Atoms in blue are peripheral nitrogen atoms that did not resonate.

The non-equivalency of $\alpha_2\beta_2$-**P·10CSA(S)** in ^{13}C and ^{15}N NMRs compared to racemic $\alpha_2\beta_2$-**P·10CSA(SR)**, shows most of the macrocyclic ring system $\Delta\sigma_{max} > 0.3$ ppm with the central two nitrogen atoms having $\Delta\sigma_{max} = 1.67$ ppm (Fig. 3 and Table S1, ESI‡). Nevertheless, due to the greater distance from the active site, most of the phenyl ring resonance signals remained isochronous. Despite this, two particularly different scenarios were portrayed by the o-Ar-^{13}C NMR signals. The $\Delta\sigma_{max}$ between 15^6 and 20^6 positions yielded excellent separation (~ 1.3 ppm), whereas the 5^6 and 10^6 imposed only marginal $\Delta\sigma_{max}$ (0.04 ppm). A closer examination of the crystal structure of $\alpha_2\beta_2$-**P**[$SO_4{}^{2-}$][$HSO_4{}^-$]$_4$ revealed a closer distance between C15^6 and C20^6 (~ 6.429 Å) than between C5^6 and C10^6 (~ 9.311 Å), subsequently forming a narrow channel for the chiral guest to occupy (Fig. 3). Moreover, the calculated chemical shifts of non-hydrogen atoms in $\alpha_2\beta_2$-**P·10CSA(R)** using the GIAO-B3LYP/6-311++G**//BP86-D3BJ/def-SVP method and SMD solvent model correlated well with the splitting patterns observed experimentally (see ESI,‡ Table S8). A comparison of the $\alpha_2\beta_2$-**P·10CSA(S** and **SR)** splitting resonance signals to other atropisomeric species is detailed in ESI‡ (Tables S2 and S3).

To conclude, the point groups play a fundamental role in adjusting supramolecular receptor systems for e.e. determinations by the NMR method. Four atropisomers containing different point group notations were thoroughly investigated by NMR with (S and R) camphorsulphonic acid pinpointing the $\alpha_2\beta_2$ rotamer as the most sensitive receptor for chirality detection. It was found that the $\Delta\sigma_{max}$ value of N–H signals can reach 0.653 ppm, a three-fold greater splitting than any known *pro*-CSA. Such enhanced sensitivity towards the chiral components allows for readily available and detailed enantiomeric excess detection at room temperature by NMR.

Conflicts of interest

There are no conflicts to declare.

References

1 (a) Z. Szakács, Z. Sánta, A. Lomoschitz and C. Szántay, *Trends Anal. Chem.*, 2018, **109**, 180–197; (b) M. S. Silva, *Molecules*, 2017, **22**, 247–268; (c) J. S. Fossey, E. V. Anslyn, W. D. G. Brittain, S. D. Bull, B. M. Chapin, C. S. Le Duff, T. D. James, G. Lees, S. Lim, J. A. C. Lloyd, C. V. Manville, D. T. Payne and K. A. Roper, *J. Chem. Educ.*, 2017, **94**, 79–84.
2 (a) J. Labuta, J. P. Hill, S. Ishihara, L. Hanyková and K. Ariga, *Acc. Chem. Res.*, 2015, **48**, 521–529; (b) A. Shundo, J. Labuta, J. P. Hill, S. Ishihara and K. Ariga, *J. Am. Chem. Soc.*, 2009, **131**, 9494–9495.
3 J. Labuta, S. Ishihara, T. Šikorský, Z. Futera, A. Shundo, L. Hanyková, J. V. Burda, K. Ariga and J. P. Hill, *Nat. Commun.*, 2013, **4**, 2188–2196.
4 (a) J. Labuta, S. Ishihara, K. Ariga and J. Hill, *Symmetry*, 2014, **6**, 345–367; (b) J. Labuta, Z. Futera, S. Ishihara, H. Kourilova, Y. Tateyama, K. Ariga and J. Hill, *J. Am. Chem. Soc.*, 2014, **136**, 2112–2118.
5 (a) J. Labuta, S. Ishihara and J. P. Hill, *J. Porphyrins Phthalocyanines*, 2020, **24**, 320–329; (b) J. Labuta, S. Ishihara, A. Shundo, S. Arai, S. Takeoka, K. Ariga and J. P. Hill, *Chem. – Eur. J.*, 2011, **17**, 3558–3561.
6 J. Labuta, S. Ishihara, D. T. Payne, K. Takimoto, H. Sato, L. Hanyková, K. Ariga and J. P. Hill, *Chemosensors*, 2021, **9**, 259–276.
7 (a) G. R. Fulmer, A. J. M. Miller, N. H. Sherden, H. E. Gottlieb, A. Nudelman, B. M. Stoltz, J. E. Bercaw and K. I. Goldberg, *Organometallics*, 2010, **29**, 2176–2179; (b) M. Balci, in *Basic 1H- and 13C-NMR Spectroscopy*, ed. M. Balci, Elsevier Science, Amsterdam, 2005, pp. 25–85.
8 J. E. Falk, in *Porphyrins and Metalloporphyrins*, ed. K. M. Smith, Elsevier Scientific Pub. Co, Amsterdam, 1975, pp. 399–514.
9 M. Roucan, M. Kielmann, S. J. Connon, S. S. R. Bernhard and M. O. Senge, *Chem. Commun.*, 2018, **54**, 26–29.
10 (a) M. Kielmann and M. O. Senge, *Angew. Chem., Int. Ed.*, 2019, **58**, 418–441; (b) K. Norvaiša, K. J. Flanagan, D. Gibbons and M. O. Senge, *Angew. Chem., Int. Ed.*, 2019, **58**, 16553–16557; (c) K. Norvaiša, M. Kielmann and M. O. Senge, *ChemBioChem*, 2020, **21**, 1793–1807.
11 (a) C. J. Kingsbury, K. J. Flanagan, H.-G. Eckhardt, M. Kielmann and M. O. Senge, *Molecules*, 2020, **25**, 3195–3218; (b) K. Norvaiša, K. Yeow, B. Twamley, M. Roucan and M. O. Senge, *Eur. J. Org. Chem.*, 2021, 1871–1882.
12 P. Bhyrappa, V. V. Borovkov and Y. Inoue, *Org. Lett.*, 2007, **9**, 433–435.
13 M. O. Senge, *Chem. Commun.*, 2006, 243–256.
14 O. S. Finikova, A. V. Cheprakov, P. J. Carroll, S. Dalosto and S. A. Vinogradov, *Inorg. Chem.*, 2002, **41**, 6944–6946.
15 C. J. Kingsbury and M. O. Senge, *Coord. Chem. Rev.*, 2021, **431**, 213760.
16 K. Norvaiša, S. Maguire, C. Donohoe, J. E. O'Brien, B. Twamley, L. C. Gomes-da-Silva and M. O. Senge, *Chem. – Eur. J.*, 2022, **28**, e202103879.
17 K. Norvaiša, J. E. O'Brien, D. J. Gibbons and M. O. Senge, *Chem. – Eur. J.*, 2020, **27**, 331–339.
18 (a) S. Ishihara, J. Labuta, Z. Futera, S. Mori, H. Sato, K. Ariga and J. P. Hill, *J. Phys. Chem. B*, 2018, **122**, 5114–5120; (b) K. Takimoto, S. Ishihara, J. Labuta, V. Březina, D. T. Payne, J. P. Hill, K. Ariga, M. Sumita, S. Mori and H. Sato, *J. Phys. Chem. Lett.*, 2020, **11**, 8164–8169.